Ultra-Wide-Band Microwave Composite Absorbers Based on Phase Gradient Metasurfaces

Yongfeng Li[1], Jiafu Wang[1, *], Jieqiu Zhang[1], Shaobo Qu[1], Yongqiang Pang[1], Lin Zheng[1], Mingbao Yan[1], Zhuo Xu[2], and Anxue Zhang[3]

Abstract—In this paper, we propose to realize ultra-wide-band absorber (UWBA) based on anomalous refraction/reflection of phase gradient metasurfaces (PGM). To achieve high absorption and meanwhile keep small thickness at low frequencies, PGM is incorporated into conventional magnetic materials (MM). The absorptivity is increased due to prolonged propagation length in the MM, which is produced via anomalous refraction/reflection mediated by the PGM. Three typical composite configurations of PGM-based absorbers are investigated and an UWBA design method is finally formulated. Due to small thickness and ultra-wide bandwidth, such absorbers possess great application potentials in EM protection, RCS reduction, etc..

1. INTRODUCTION

Conventional magnetic materials (MMs) are usually effective absorbers for microwaves [1–3]. Wide-band absorption can be achieved using MMs. However, when the MMs are used as absorbers in lower frequency band, especially in L-band, large thickness is always necessary. This makes MM absorbers very heavy and bulky, which curbs their practical applications. Besides, metamaterials can also be used to realize absorbers at microwave and optical frequencies [4–8]. As used as low frequency absorbers, single-layer metamaterial absorbers are usually narrowband. In this regard, a composite absorber (CA) based on the MM and ultra-thin phase gradient metasurface (PGM) is proposed to improve the low frequency absorptivity.

Phase gradient metasurface (PGM) is an anisotropic artificial surface with sub-wavelength thickness [9–19]. Generally, it is formed by spatial arrangement of different metallic unit cells within sub-wavelength dimensions. The PGM provides an approach to control the propagation of electromagnetic wave (EMW) with much more freedom. It is realized according to the generalized reflection law or refraction law (Snell's Law). The PGM is firstly proposed and achieved using V-shaped antenna by Yu et al. in 2011 [9]. Waveplate and flat lens etc were achieved in their subsequent works [10–13]. Sun et al. achieved a surface electromagnetic wave (SEMW) coupler by a reflective PGM using "H" shaped metallic unit cells as the sub-unit resonators [14]. A high efficiency anomalous refraction is realized by a PGM on the basis of a high-efficiency linear-polarization conversion metamaterial [15]. In their works, the incident linearly polarized wave is highly abnormally transmitted and converted into wave polarized on its orthogonal direction. Huang et al. realized dispersionless phase gradient under circularly polarized wave incidence. Based on the dispersionless phase gradients, wideband anomalous refraction and surface wave excitation are realized, respectively [16, 17]. In our previous researches, a reflective PGM is presented by the split resonator rings (SRR) to serve as a SEMW coupler for a

* Corresponding author: Jiafu Wang (wangjiafu1981@126.com).
[1] College of Science, Air Force Engineering University, Xi'an 710051, People's Republic of China. [2] Electronic Materials Research Laboratory, Key Laboratory of Ministry of Education, Xi'an Jiaotong University, Xi'an 710049, People's Republic of China. [3] School of Electronics & Information Engineering, Xi'an Jiaotong University, Xi'an, Shaanxi 710049, People's Republic of China.

specific polarized incident wave [18]. A two-dimensional reflective PGM is designed for wide-band RCS reduction due to the anomalous reflection, surface wave coupling and diffusion [19].

The absorption properties of the MMs in low frequency (especially in L and S frequency-band) always suffer from larger thickness and limited absorptivity. In this paper, a composite absorber (CA) consisted of conventional MM and ultra-thin PGM is proposed to improve the absorption property at lower frequency. The ultra-thin PGM makes the incident waves be abnormally refracted/reflected or coupled into SEMW propagating along the PGM. In this case, the propagation distance in the MM for the incident wave is greatly increased compared with the single MM absorber with the same thickness. In other words, this CA can be regarded as a MM absorber with increased thickness. Consequently, this CA can greatly reduce the thickness of the lower frequency absorber and improve its absorption efficiency effectively. Three typical CAs were proposed, for which the absorption property was simulated and analyzed. Ultimately, an ultra-wide-band CA is proposed.

2. THE WORKING PRINCIPLE OF THE COMPOSITE ABSORBER

Figure 1 gives the working principle diagram of the proposed CA, where Figures (a), (b) are for anomalous refraction and anomalous reflection, and (c), (d) describe the SEMW coupling as the EMW incidents onto the PGM. The CA is composed of a conventional MM, a covered ultra-thin PGM and the metal back-sheet. The thickness of the MM is d. According to the generalized versions of reflection law and refraction law, the anomalous reflection/refraction angle θ can be calculated using $\theta = \arcsin(\nabla\Phi/k_0)$ for the normal incident wave, where $\nabla\Phi$ is the phase gradient of the PGM, and k_0 is the wavevector of the incident wave in free space. The equivalent propagation distance of the anomalously reflected wave in the MM is $d_e = d/\cos(\theta)$. When the anomalously refracted/reflected angle is greater than 90 degree, the wave is coupled into SEMW and an infinite equivalent propagation distance is obtained. Thus, this CA can be approximately considered as a MM absorber within an increased thickness. In detail, for (a) and (b), as a beam of EMW is normally incident onto the CA, a part of the transmitted wave is abnormally refracted into the MM [see Figure 1(a)], and the other is reflected by the metal backsheet and then anomalously reflected into the MM again by the PGM,
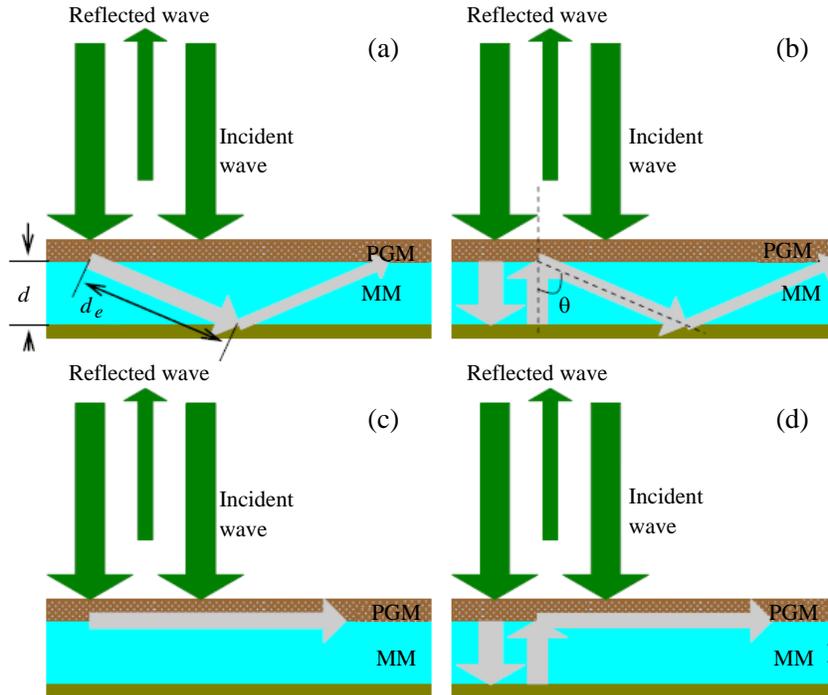
Figure 1. The working principle diagram for the proposed CA composed of MM and PGM.

as shown Figure 1(b), For Figures (c) and (d), a part of the normally incident waves is coupled into SEMWs propagating along the PGM (c), the other normally transmitted waves is reflected by the metal backsheet and then coupled into SEMWs propagating along the PGM (d).

We use t and r to denote the anomalous transmission coefficient and reflection coefficient for the PGM, respectively. A is the absorption coefficient of the single MM absorber consisted of the MM and a metal backsheet. Suppose that the anomalously transmitted and reflected waves are completely absorbed by the MM. The absorption coefficient of the CA can be approximately derived from the following expression,

$$A_c = r + t + A(1 - t - r - r_n) + (1 - t - r - r_n)(1 - A)r \tag{1}$$

where r and t represent the anomalously reflected and refracted waves; $(1 - t - r - r_n)A$ is absorption of the normally transmitted waves by MM; $(1 - t - r - r_n)(1 - A)r$ depicts the anomalously reflected waves for the normally transmitted waves reflected by the metal backsheet.

3. DESIGN OF THE PHASE GRADIENT METASURFACE

For simplicity, a circularly polarized transmissive PGM is designed. Under linearly polarized wave incidence, the anomalously reflected and refracted waves are all divided into two beams of circularly polarized waves propagating along opposite directions due to the opposite phase gradient for left-handed and right-handed circular polarization (LCP and RCP) waves incidence. The PGM is achieved using a circular polarization conversion metasurface unit cell as the basic sub-unit resonators. Figure 2(a) shows the schematic view of the unit cell for the circular polarization conversion metasurface, which is composed by a metallic pattern arrays printed on a FR4 ($\varepsilon_r = 4.3$, $\tan\delta = 0.025$) dielectric substrate. The optimized values of the dimension parameters depicted in figure are all given in the options of Figure 2. Figure 2(b) gives the simulated polarization conversion ratios (PCR) for reflection and transmission under circular polarization (CP) wave incidence. The polarization conversion ratio (PCR) for reflection and transmission are defined as $PCR_r = (r_{LR(RL)}^2/(r_{LR(RL)}^2 + r_{LL(RR)}^2 + t_{LR(RL)}^2 + t_{LL(RR)}^2))$ and $PCR_t = (t_{LR(RL)}^2/(r_{LR(RL)}^2 + r_{LL(RR)}^2 + t_{LR(RL)}^2 + t_{LL(RR)}^2))$, respectively, where $r_{LR(RL)}$ and $r_{LL(RR)}$ denote the cross-polarization and co-polarization reflections under LCP and RCP waves incidence, respectively. Similarly, $t_{LR(RL)}$ and $t_{LL(RR)}$ represent the cross-polarization and co-polarization transmissions under LCP and RCP waves incidence, respectively. From the figure, we can find that the PCR for reflection and transmission under circular polarization wave incidence are all greater than 16.5% over a wide frequency range from 1 GHz to 6 GHz.
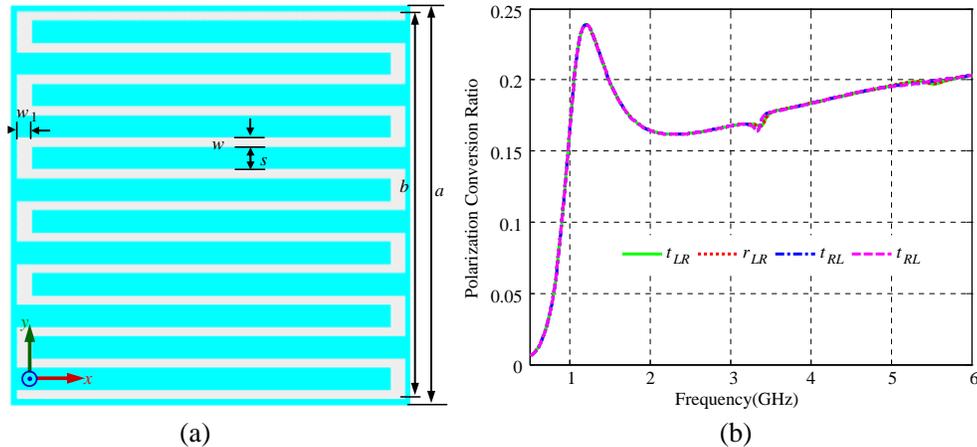
Figure 2. (a) The front view of the circular polarization conversion metasurface and (b) the simulated PCR of reflection and transmission under CP waves incidence, where the optimized values of the dimension parameters are: $a = 12.41$ mm, $b = 12.01$ mm, $w = 0.28$ mm, $w_1 = 0.46$ mm and $s = 0.73$ mm.

Based on the unit cells of the polarization conversion metasurface, a phase shift $\triangle\Phi$ of the polarization conversion coefficient can be produced by rotating the unit cell by α degree in-plane (xoy plane), where $\triangle\Phi = \pm 2\alpha$, signs "+" and "−" are corresponding to the LCP and RCP wave incidence, respectively. Thus, arbitrary dispersionless phase gradient can be achieved by $\nabla\Phi = \pm 2\alpha/a$, where a is the repetition period of the sub-unit cells. In this paper, we designed a two-dimensional PGM using four different polarization conversion metasurface unit cells. Figure 3 shows the front view of the super-unit of the designed PGM. The phase differences between adjacent sub-unit cells are π and hence the super-unit realizes a total 4π phase shift along x- and y-directions, respectively. $\nabla\Phi_x$ and $\nabla\Phi_y$ represent the phase gradients in x and y-directions and have the same values $\pm\pi/a$. To verify the phase gradient designation, we simulated the amplitudes and phases of the polarization conversion reflections and transmissions for LCP wave incident onto these four different sub-unit cells used in the
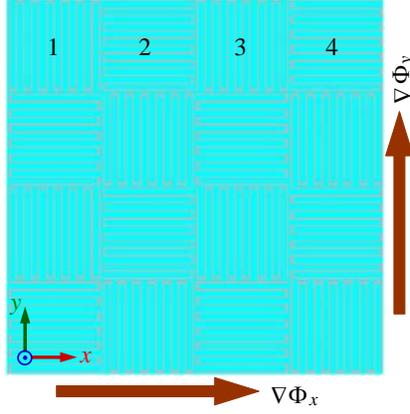
Figure 3. The schematic view of the super-unit for the designed PGM.
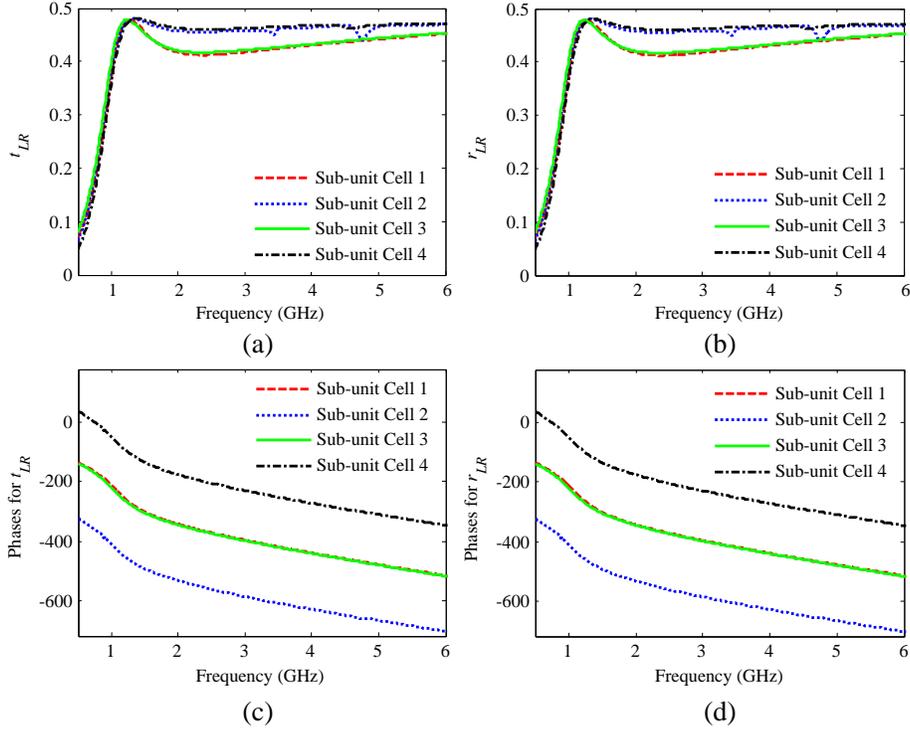
Figure 4. The simulated amplitudes and phases of the cross-polarization transmissions and cross-polarization reflections for the used four sub-unit cells in super unit.
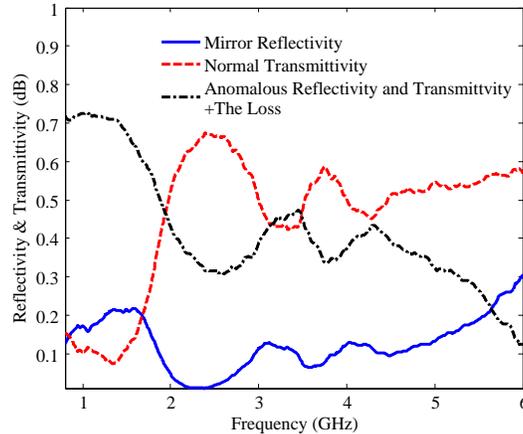
Figure 5. The simulated mirror reflectivity and normal transmissivity.

super-unit. The four sub-unit cells are denoted using the serial numbers 1, 2, 3 and 4 as shown in Figure 3. The simulated results are given in Figure 4. In Figure 4, the Sub-figures (a) and (b) give the amplitudes of the cross-polarization transmissions and reflections of the four sub-unit cells under LCP wave normal incidence. It is observed that the amplitudes are all greater than 0.4 over a wide frequency range from 1.0 GHz to 6.0 GHz. The Sub-figures (c) and (d) give the phases of the cross-polarization transmissions and reflections of the four sub-unit cells under LCP wave incidence. It can be found that the phase-shifts between adjacent sub-unit cells are approximately equal to π in the whole simulated frequency band.

In addition, we perform numerical simulation using CST microwave studio to calculate the mirror reflectivity and normal transmissivity under linearly polarized wave normal incidence. The results are given in Figure 5. The total energy including the anomalous reflectivity, anomalous transmissivity and the loss can be extracted from the simulated results. Under linearly polarized wave incidence, part of the incident wave is anomalously reflected into two beams of CP waves (LCP and RCP waves) propagating along opposite directions and part of the incident wave is anomalously refracted into two beams of CP waves propagating along opposite directions. Therefore, the total energy of mirror reflectivity and normal transmissivity is greatly reduced compared with the energy of the incident wave. The anomalous reflectivity and transmissivity are well consistent with the polarization conversion reflection and transmission at the frequency range 1.0–6.0 GHz.

4. ACHIEVEMENT OF THE COMPOSITE ABSORBER

4.1. Absorbing Property of MM (ECCOSORB SFU-2)

Conventional MM absorber has excellent absorbing property at high microwave frequency and always wide-band absorbing property. However, as the MM is used at low frequencies, the large thickness, bulk configuration, great weight and limited absorptivity impede its adoption. As an example, the absorbing property of the MM ECCOSORB SFU-2 backed by a metal backsheet is numerically simulated using the CST Microwave Studio. The calculated reflectivities with different thickness of MM are given in Figure 6. It is observed that the reflectivity tip moves towards lower frequency with increasing thickness of the MM. However, with increasing the thickness of the MM, in lower frequency band, especially in L-band, the reflectivity improvement is very small. For the 3 mm-thick MM, the reflectivity is below -5 dB over the frequency range from 0.45 GHz to 3.5 GHz.

4.2. Achievement of the Composite Absorber

Based on the ultra-thin PGM designed in Section 3, three typical CAs (denoted as CA-1, CA-2, and CA-3) consisting of PGM and MMs were proposed as shown in Figure 7. We firstly designed a composite absorber (CA-1) as shown in Figure 7(a). It is composed by covering the ultra-thin PGM on the top of the MM absorber. ECCOSORB SFU-2 is chose as the conventional MM and d_1 represents
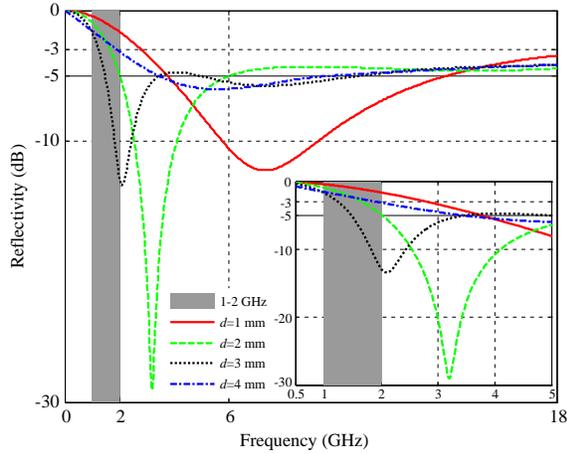
Figure 6. The reflectivity versus frequency of the MM (ECCOSORB SF-2) absorber with different thickness of the MM.
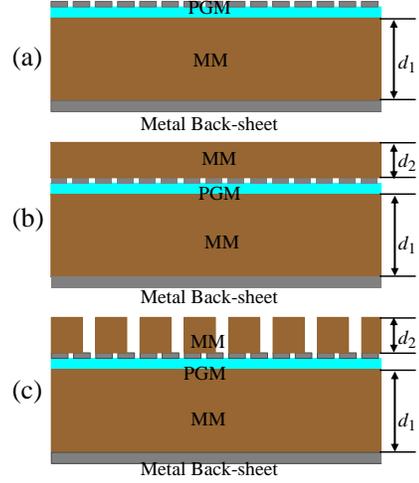
Figure 7. The proposed three typical CAs (CA-1, CA-2 and CA-3) composed by MMs and the ultra-thin PGM.
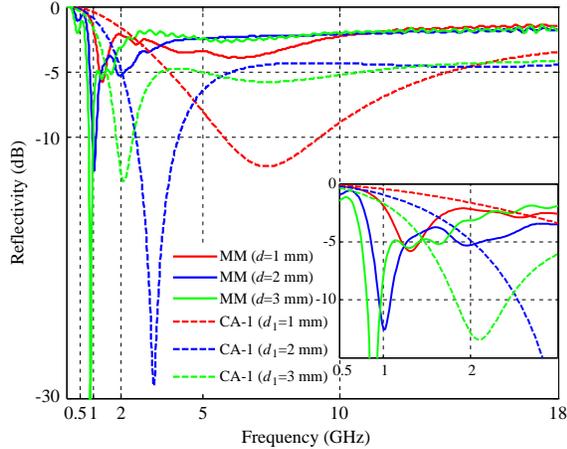
Figure 8. The reflectivities of CA-1 and the only MM absorber with the same thickness.
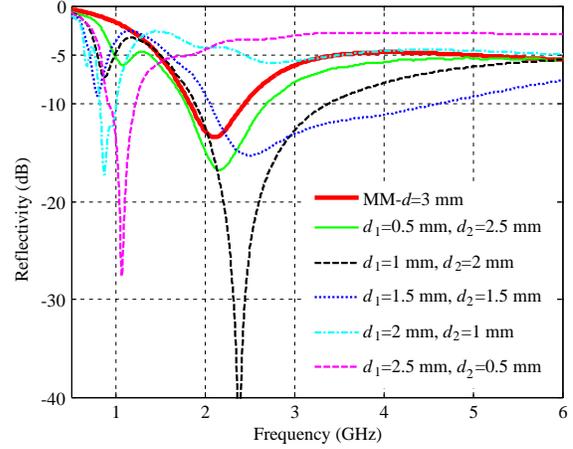
Figure 9. The simulated reflectivity of the CA-2 with different thickness of the bottom layer of MM d_1, the total thickness of the MMs used in CA-2 is fixed to be $d_t = 3$ mm.

its thickness. As for CA-1, we perform numerical simulations to calculate the reflectivity for TM wave normal incidence. The simulated results with different thicknesses d_1 of the MM are given in Figure 8. For comparison, the reflectivity of the MM absorber with different thicknesses d are also simulated and given by the dotted lines in Figure 8. The inset gives a zoom view of the reflectivity at the frequency range 0.5–3 GHz. Obviously, at low frequencies, the simulated reflectivity decreases with increasing thickness of the MM d_1 and the absorbing frequency shifts towards to the lower frequency. The reflectivity of the CA-1 highly decreases compared with the only MM absorber with the same thickness. In detail, when the thickness of the MM is $d_1 = 3$ mm, the reflectivity of CA-1 less than -5 dBb covers a wide frequency range 0.75–1.7 GHz, and the reflectivity dip is as low as -20 dB at 0.85 GHz. This mainly attributes to the SEMW coupling as the wave is incident onto the covered PGM. An enlarged propagation distance is resulted. However, at the high frequency range, the absorbing property becomes poor, that the reflectivity of the CA-1 is almost higher than -3 dB in the frequency range 3.0–18.0 GHz, being much greater than the reflectivity of the only MM absorber with the same thickness. This is because the matching of the origin MM to the free space collapsed due to the existence of the covered PGM.

In order to improve the absorbing property at the high frequencies, the second CA (CA-2) consisted

of the CA-1 and a top covered MM with the thickness d_2 is proposed, as shown in Figure 7(b). ECCOSORB SFU-2 is also used as the top layer MM. The total thickness of the two layers of MMs is $d_t = d_1 + d_2$. In this case, the matching between the CA-2 and the free space at high frequencies will be improved compare with CA-1. In order to verify our analysis, we performed numerical simulations to calculate the reflectivity of CA-2 with different thickness of the bottom layer of MM d_1 ($d_1 = 0.5$, 1, 1.5, 2 and 2.5 mm) under TM waves normal incidence. The total thickness of the MMs is fixed to be $d_t = 3$ mm and the simulated results are given in Figure 9. For comparison, the reflectivity of the only 3 mm-thick MM is also given using a red line in Figure 9. It is observed that the reflectivity of CA-2 decreases with increasing thickness of the bottom layer of MM at low frequencies. Compare with the 3 mm-thick MM absorber, the absorptivity at low frequencies are all greatly improved. In the high frequency range, the absorptivity is also improved compare with the 3 mm-thick MM absorber when the thickness of the bottom layer MM d_1 is less than 1 mm, yet the reflectivity increases with increasing d_1 as the thickness of the bottom layer MM d_1 is greater than 1 mm. We can find that there is nearly no improvement for the absorbing property of the CA-2 in the high frequency band with respect to the CA-1. It is worth to be mentioned that the low frequency absorbing property is affected because of the added top layer of MM compared with the CA-1 of the same thickness.

As we know, the proposed CA-1 has a good performance in low frequency band. However, the high frequency absorbing property becomes poor because of mismatching between the covered PGM and the free space. In order to simultaneously consider the high frequency absorption, CA-2 is proposed to add a top layer MM onto CA-1 to improve the matching. But the lower frequency absorbing property is deteriorated. In order to further improve the absorbing property of the CA-2, we proposed anther CA (denoted as CA-3) on the basis of CA-2 as shown in Figure 7(c). The front view of CA-3 is given in Figure 10, in which the top layer MM is optimized to be periodically arranged MM patches. The side-length of the MM patch is optimized to be $c = 11.2$ mm. Its thickness is d_2, and the total thickness of the two layers of MMs is $d_t = d_1 + d_2$. The repetition period of the MM patch is equivalent to that of the sub-units of the PGM, and the side length of the MM patch is $c = 5.6$ mm. To study the absorbing property of CA-3, the reflectivity of the CA-3 with different thicknesses of the bottom layer MM d_1 together with the only 3 mm-thick MM absorber under TM wave normal incidence is simulated, and the results are given in Figure 11. The total thickness of the two layers of MMs d_t is fixed to be 3 mm. From the figure, we can find that in the lower frequency band, the reflectivity decreases with increasing thickness d_1, and the absorbing properties are all greatly improved compared with the 3 mm-thick MM absorber depicted by the bold red-line. At the high frequency range $f > 3$ GHz, the reflectivity of the CA-3 are all less than that for the only MM absorber if the thickness of the bottom layer MM $d_1 < 2.5$ mm.

Taking the CA-3 ($d_1 = 2$ mm, $d_2 = 1$ mm) as an example, the simulated reflectivity is below -6.5 dB
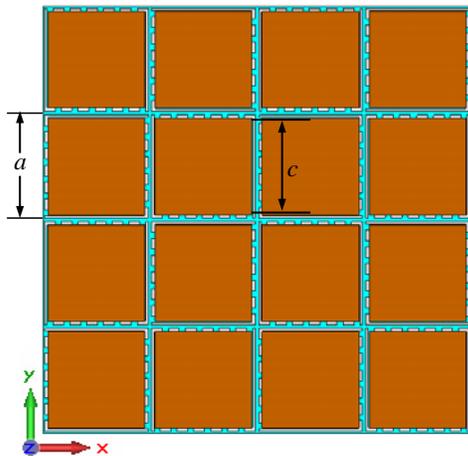
Figure 10. The front view of the CA-3, in which the side length of the MM-patch $c = 11.2$ mm.
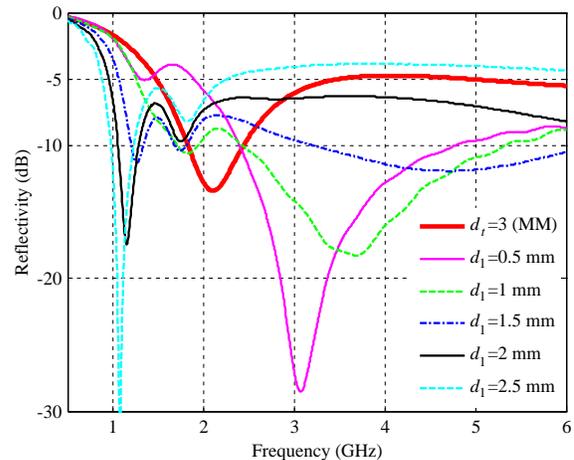
Figure 11. The simulated reflectivity for the CA-3 with different thickness of the bottom layer MM d_1 for TM wave normal incidence.

over a wide frequency range from 1.0 GHz to 6.0 GHz. The lowest reflectivity is as low as -17 dB at the frequency $f = 1.164$ GHz. In order to get an intuitive view of the absorbing principle, the distributions of the electromagnetic fields at frequency $f = 1.164$ GHz under TM wave normal incidence is simulated, and the results are given in Figure 12. It is observed that at frequency $f = 1.146$ GHz, the incident field is highly localized near the surface of the PGM. Part of the incident wave is coupled into two beams of SEMW propagating along the surface of the PGM due to the compensated greater phase gradient provided by the PGM. The two beams of coupled SEMWs propagate along opposite directions at the PGM and attenuate in the process of the propagation. Figure 13 gives the simulated power flow at the frequency $f = 1.164$ GHz corresponding with Figure 12. The given inset is a zoom view of the simulated power flow. From the figure, we can find that as the incident TM wave transmits through the PGM of the CA-3, the power flow is divided into two parts in two opposite directions at x-direction in the bottom MM.

In order to make a comparison between the four absorbers: the only MM absorber ($d_1 = 3$ mm), the composite absorber CA-1 ($d_1 = 3$ mm), CA-2 ($d_1 = 2$ mm, $d_2 = 1$ mm) and CA-3 ($d_1 = 2$ mm, $d_2 = 1$ mm). The simulated reflectivities versus frequency from 0.5 GHz to 6.0 GHz of the four absorbers under TM waves incidence are given in Figure 14. Compared with the only 3 mm-thick MM absorber, the absorbing properties in low frequency regime are all improved. Over the frequency range 3.0–6.0 GHz, the absorptivities of the CA-2 and CA-3 have been greatly improved, and that for CA-1 becomes worse than that for only MM absorber. Considering the absorbing properties both in low and high frequency regimes, the CA-3 has the best performance. As for the CA-3 ($d_1 = 2$ mm, $d_2 = 1$ mm), using ECCOSORB SFU-9.5 to substitute ECCOSORB SFU-2 for the top layer MM-patch array, which has better performance in absorbing at high frequencies, and the absorbing property in high frequency regime will be further enhanced. The simulated reflectivity under TM wave normal incidence is given in Figure 15. It can be seen that the reflectivity is approximately less than -5 dB over the whole frequency range from 1.0 GHz to 18.0 GHz and is below -10 dB at the frequency range 12.0–18 GHz.
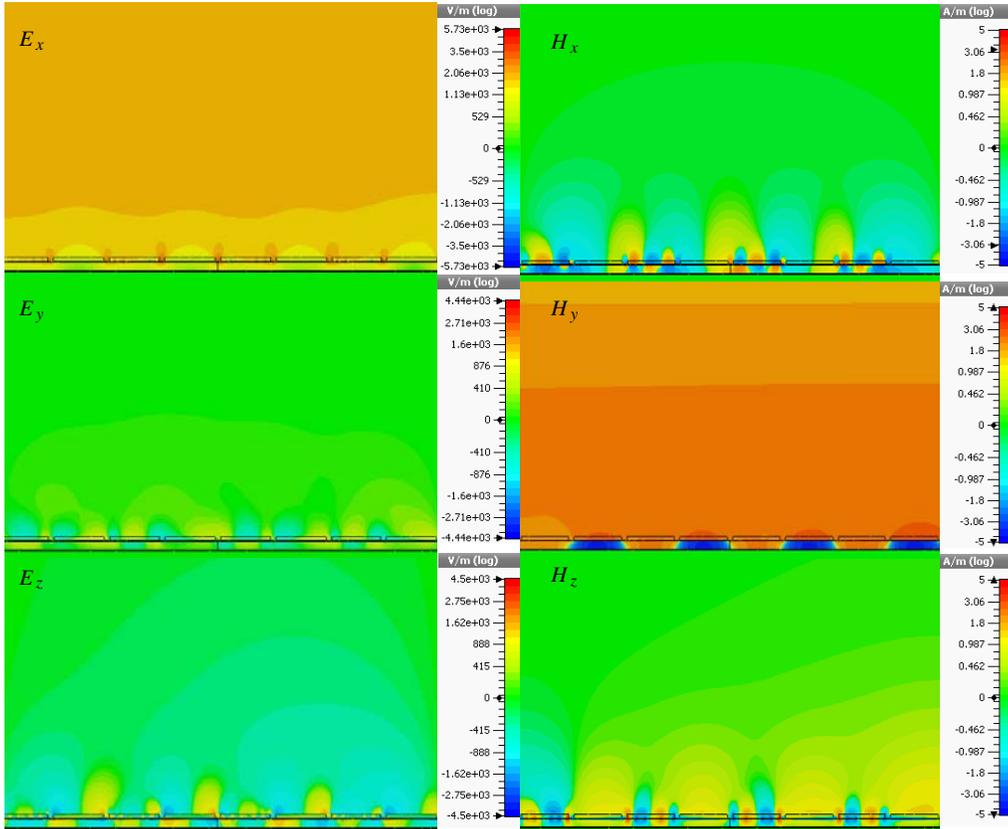
Figure 12. The distributions of the electromagnetic fields at $f = 1.164$ GHz for TM wave normal incidence.
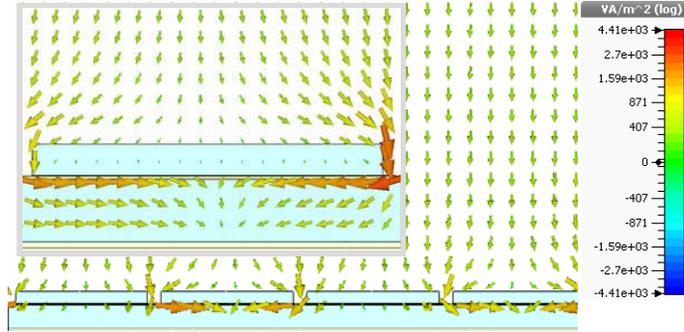
Figure 13. The simulated power flow at $f = 1.164\,\text{GHz}$ for TM wave normal incidence onto the CA-3 ($d_1 = 2\,\text{mm}$, $d_2 = 1\,\text{mm}$), the inset is a zoom view.
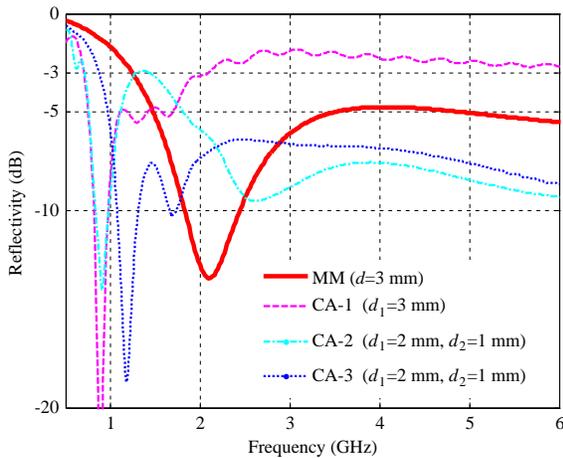
Figure 14. The reflectivity of the four different absorbers with the same total thickness of MMs (the only MM absorber, CA-1, CA-2 and CA-3).
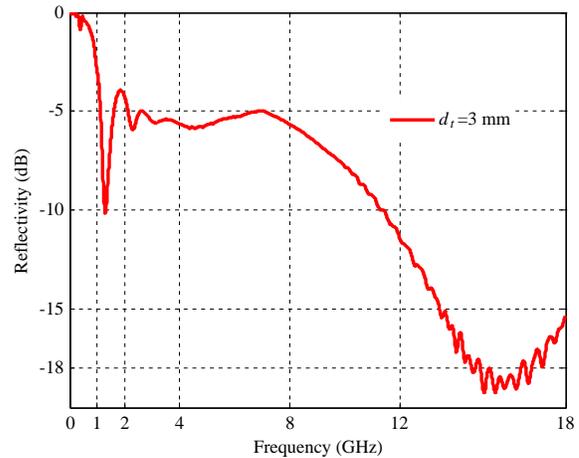
Figure 15. The simulated reflectivity of the CA-3 ($d_1 = 2\,\text{mm}$, $d_2 = 1\,\text{mm}$), in which SFU9-5 instead of SFU-2 as the top layer MM.

5. CONCLUSION

In summary, the composite absorber consisting of conventional MMs and ultra-thin PGM is proposed to improve the absorbing property at low frequency regime. As illuminated by the linearly polarized waves, the incident wave is partially anomalously reflected/refracted into the MM or coupled into SEMW propagating along the PGM. Thus an equivalently extended propagation distance in MM is obtained, and the CA can be considered as the MM with increased thickness. In this paper, three typical composite absorbers (CA-1, CA-2, and CA-3) are proposed and studied. In detail, the CA-1 is proposed to improve the absorbing property at low frequencies, and the CA-2 is proposed by the CA-1 and a covered layer of MM to buildup matching between the composite absorber and the free space in the high frequency regime. To improve the absorbing property in both low and high frequency regimes, the CA-3 is proposed. Ultimately, an ultra-wide-band (1–18 GHz) composite absorber is realized by the CA-3, in which different MMs are used for the two layers of MMs.

REFERENCES

1. Meshram, M. R., N. K. Agrawal, B. Sinha, and P. S. Misra, "Characterization of M-type barium hexagonal ferrite-based wide band microwave absorber," *J. Magn. Magn. Mater.*, Vol. 271, 207–214, 2004.

2. Politano, A. and G. Chiarello, "Plasmon modes in graphene: Status and prospect," *Nanoscale*, Vol. 6, 10927–10940, 2014.

3. Politano, A. and G. Chiarello, "Collective electronic excitations in systems exhibiting quantum well states," *Surf. Rev. Lett.*, Vol. 16, 171–190, 2009.

4. Cao, Z. X., F. G. Yuan, and L. H. Li, "A super-compact metamaterial absorber cell in L-band," *Journal of Applied Physics*, Vol. 115, 184904, 2014.

5. Tuong, P. V., D. L. Vu, J. W. Park, and Y. Lee, "Polarization-controlling dual-band absorption metamaterial," *Adv. Nat. Sci: Nanosci. Nanotechnol.*, Vol. 4, 035009, 2013.

6. Huang, L. and H. Chen, "Multi-band and polarization insensitive metamaterial absorber," *Progress In Electromagnetics Research*, Vol. 113, 103–110, 2011.

7. Zhu, B., Z. Wang, C. Huang, Y. J. Feng, J. Zhao, and T. Jiang, "Polarization insensitive metamaterial absorber with wide incident angle," *Progress In Electromagnetics Research*, Vol. 101, 231–239, 2010.

8. Landy, N. I., S. Sajuyigbe, J. J. Mock, D. R. Smith, and W. J. Padilla, "Perfect metamaterial absorber," *Phys. Rev. Lett.*, Vol. 100, 2074021–2074024, 2008.

9. Yu, N., P. Genevet, M. A. Kats, F. Aieta, J.-P. Tetienne, F. Capasso, and Z. Gaburro, "Light propagation with phase discontinuities: Generalized laws of reflection and refraction," *Science*, Vol. 334, 333–337, 2011.

10. Aieta, F., P. Genevet, N. Yu, M. A. Kats, Z. Gaburro, and F. Capasso, "Out-of-plane reflection and refraction of light by anisotropic optical antennas metasurfaces with phase discontinuities," *Nano Lett.*, Vol. 12, 1702–1706, 2012.

11. Aieta, F., P. Genevet, M. A. Kats, N. Yu, R. Blanchard, Z. Gaburro, and F. Capasso, "Aberration-free ultrathin flat lenses and axicons at telecom wavelengths based on plasmonic metasurfaces," *Nano Lett.*, Vol. 12, 4932–4936, 2012.

12. Yu, N., F. Aieta, P. Genevet, M. A. Kats, Z. Gaburro, and F. Capasso, "A broadband, background-free quarter-wave plate based on plasmonic metasurfaces," *Nano Lett.*, Vol. 12, 6328–6333, 2012.

13. Roberts, A. and L. Lin, "Plasmonic quarter-wave plate," *Opt. Lett.*, Vol. 37, 1820–1822, 2012.

14. Sun, S., Q. He, S. Xiao, Q. Xu, X. Li, and L. Zhou, "Gradient-index meta-surfaces as a bridge linking propagating waves and surface waves," *Nat. Mater.*, Vol. 11, 426–431, 2012.

15. Grady, N. K., J. E. Heyes, D. R. Chowdhury, Y. Zeng, M. T. Reiten, A. K. Azad, A. J. Taylor, D. A. R. Dalvit, and H. T. Chen, "Terahertz metamaterials for linear polarization conversion and anomalous refraction," *Science*, Vol. 340, 1304, 2013.

16. Chen, X., L. Huang, H. Mühlenbernd, G. Li, B. Bai, Q. Tan, G. Jin, C.-W. Qiu, T. Zentgraf, and S. Zhang, "Reversible three-dimensional focusing of visible light with ultrathin plasmonic flat lens," *Adv. Optical Mater.*, Vol. 1, 517–521, 2013.

17. Huang, L., X. Chen, B. Bai, Q. Tan, G. Jin, T. Zentgraf, and S. Zhang, "Helicity dependent directional surface plasmon polariton excitation using a metasurface with interfacial phase discontinuity," *Light: Sci. Applications*, Vol. 2, e70, 2013.

18. Wang, J. F., S. B. Qu, H. Ma, Z. Xu, A. X. Zhang, H. Zhou, H. Y. Chen, and Y. F. Li, "High-efficiency spoof plasmon polariton coupler mediated by gradient metasurfaces," *Appl. Phys. Lett.*, Vol. 101, 201104, 2012.

19. Li, Y. F., J. Q. Zhang, S. B. Qu, J. F. Wang, H. Y. Chen, Z. Xu, and A. X. Zhang, "Wideband radar cross section reduction using two-dimensional phase gradient metasurface," *Appl. Phys. Lett.*, Vol. 104, 221110, 2014.